

THE MIRA-TITAN UNIVERSE II: MATTER POWER SPECTRUM EMULATION

EARL LAWRENCE¹, KATRIN HEITMANN^{2,3}, JULIANA KWAN^{4,5}, AMOL UPADHYE⁶, DEREK BINGHAM⁷,
SALMAN HABIB^{2,3}, DAVID HIGDON⁸, ADRIAN POPE⁹, HAL FINKEL⁹, NICHOLAS FRONTIERE^{2,10}

¹ CCS-6, CCS Division, Los Alamos National Laboratory, Los Alamos, NM 87545, USA

² HEP Division, Argonne National Laboratory, Lemont, IL 60439, USA

³ MCS Division, Argonne National Laboratory, Lemont, IL 60439, USA

⁴ Kavli Institute for the Physics and Mathematics of the Universe (Kavli IPMU, WPI), Todai Institutes for Advanced Study, the University of Tokyo, Kashiwa, Chiba 277-8583, Japan

⁵ Department of Physics and Astronomy, University of Pennsylvania, Philadelphia, PA 19104, USA

⁶ Department of Physics, University of Wisconsin-Madison, Madison, WI 53706, USA

⁷ Department of Statistics and Actuarial Science, Simon Fraser University, Burnaby, BC, Canada

⁸ Social and Decision Analytics Laboratory, Virginia Bioinformatics Institute, Virginia Tech, Arlington, VA 22203, USA

⁹ ALCF Division, Argonne National Laboratory, Lemont, IL 60439, USA

¹⁰ Department of Physics, University of Chicago, Chicago, IL 60637, USA

Draft version May 10, 2017

ABSTRACT

We introduce a new cosmic emulator for the matter power spectrum covering eight cosmological parameters. Targeted at optical surveys, the emulator provides accurate predictions out to a wavenumber $k \sim 5\text{Mpc}^{-1}$ and redshift $z \leq 2$. Besides covering the standard set of ΛCDM parameters, massive neutrinos and a dynamical dark energy of state are included. The emulator is built on a sample set of 36 cosmological models, carefully chosen to provide accurate predictions over the wide and large parameter space. For each model, we have performed a high-resolution simulation, augmented with sixteen medium-resolution simulations and TimeRG perturbation theory results to provide accurate coverage of a wide k -range; the dataset generated as part of this project is more than 1.2Pbyte. With the current set of simulated models, we achieve an accuracy of approximately 4%. Because the sampling approach used here has established convergence and error-control properties, follow-on results with more than a hundred cosmological models will soon achieve $\sim 1\%$ accuracy. We compare our approach with other prediction schemes that are based on halo model ideas and remapping approaches. The new emulator code is publicly available.

Subject headings: methods: statistical — cosmology: large-scale structure of the universe

1. INTRODUCTION

The field of cosmology has undergone a remarkable transformation in the last two decades – from a somewhat qualitative picture of the make-up and evolution of the Universe we have arrived at the ‘Standard Model’ of cosmology with parameters constrained at the few percent level (Ade et al. 2015; Anderson et al. 2014). Despite the phenomenological and descriptive success of the Standard Model, many foundational questions still require answers. Our understanding of the fundamental physics is lacking in critical areas: We do not properly understand the cause of the accelerated expansion of the Universe (Caldwell & Kamionkowski 2009), the nature of dark matter is unknown (Feng 2010), and our understanding of the physics of inflation remains incomplete, to mention three of the most prominent puzzles. Ongoing and upcoming cosmological surveys and experiments aim to address these and other questions by providing datasets with much smaller statistical errors and extended range in spatial scales and redshift. Analysis of these observations can provide important clues by providing evidence against a cosmological constant, or even against general relativity as the preferred theory of gravity (Joyce et al. 2015). Some of the data will put added constraints on the properties of dark matter candidates, and also significantly tighten the current cosmological errors on determining the sum of neutrino masses. Because of the enhancement of data quality, it is therefore important – from a theoretical and modeling perspective – to open up new parameters beyond the standard set

of $\theta = \{\omega_{cdm}, \omega_b, \sigma_8, h, n_s\}$ and also enter new uncharted areas with respect to length scales, exploring nonlinear regimes that might provide new insights into the dynamics of the Universe.

In order to take full advantage of the new data, and not be theory/modeling-limited, prediction tools must be available at accuracy levels significantly better than those characteristic of the measurements. Since surveys increasingly probe the nonlinear regime of structure formation, theoretical predictions have to be derived from detailed and error-controlled simulations that are necessarily computationally expensive. While this may be a reasonable approach to study individual models, it is not practical as a tool for exploring parameter space, nor does it help in solving the cosmological inverse problem of determining parameters based on observational knowledge of a set of summary statistics, where hundreds of thousands to millions of forward model evaluations may be needed.

In order to address the above requirement, we have embarked on a program to create very fast oracles, or “cosmic emulators” for various cosmic probes. The aim of the approach is to achieve robustly accurate prediction schemes over a range of cosmological parameters, based on a relatively small number of underlying simulations. The complete framework not only provides predictions for specific cosmological statistics but also includes a self-contained Bayesian inference engine to constrain cosmological parameters by combining observational data and emulator predictions (‘cosmic calibration’). We first introduced the concept in Heitmann et al. (2006) based on a set of lower resolution gravity-only simulations and a

simulated data set for the nonlinear matter power spectrum. In a second paper, Habib et al. (2007), we extended the approach to include measurements for the cosmic microwave background (CMB). In a following set of four papers (Heitmann et al. 2010, 2009; Lawrence et al. 2010; Heitmann et al. 2014), the Coyote Universe series, we focused on providing a high-accuracy prediction tool for the matter power spectrum over a range of six cosmological parameters, adding w to the standard set of five. Later, we added other emulators to predict the halo concentration-mass relation (Kwan et al. 2013) and the galaxy power spectrum, using halo occupation distribution (HOD) modeling (Kwan et al. 2015).

In this paper, we focus again on the matter power spectrum, while extending the range of cosmological parameters to eight, $\theta = \{\omega_{cdm}, \omega_b, \sigma_8, h, n_s, w_0, w_a, \omega_\nu\}$ and employing higher-quality simulations than in the original Coyote Universe, simultaneously improving on the mass resolution and the simulation volume. This work builds on the convergent sampling strategy described in Heitmann et al. (2015) to systematically improve emulation accuracy by adding new simulations to a previous sample, following Bergner (2011). In the original work, the idea was demonstrated on a set of linear power spectra as well as for mass function predictions (assuming universality of the mass function across cosmologies, which is valid at the 5-10% level) – we now release the first nonlinear emulator from the Mira-Titan Universe simulation suite. The inclusion of a dynamical dark energy component and massive neutrinos is non-trivial – the approach to the simulations is described in more detail in Heitmann et al. (2015). Several tests of the simulation methodology were carried out in Upadhye et al. (2014), where results on large scales were compared to TimeRG perturbation theory. Discussions of the range of validity and methods for adding baryonic corrections are provided in Section 3.1.

The eventual aim of the emulators constructed from the Mira-Titan Universe simulation suite is to reach simulation prediction accuracies at the 1% level, which requires results for more than a hundred cosmological models. The sampling strategy followed allows us to make emulators at intermediate accuracy levels before all the simulations are completed and to check thereby that the appropriate accuracies are in fact being achieved during this process. (This also includes demonstrating successful data filtering, data reduction with principal components, and finally, Gaussian process modeling to carry out the required interpolation.) Results presented in this paper demonstrate the success of this strategy.

Several other approaches have been suggested to provide predictions for the matter power spectrum going beyond Λ CDM. Agarwal et al. (2014) included neutrinos and constructed an emulator using machine learning techniques. Takahashi et al. (2012) used a set of simulations to improve the original Halofit predictions and Bird et al. (2012) added a neutrino contribution to this model. Casarini et al. (2016) used an approximate approach to extend the Coyote Universe emulator to include w_a as a new parameter, in order to cover the model space of dynamical dark energy models. Finally, Mead et al. (2016) used a halo model approach to include effects of neutrinos, modified gravity, and dynamical dark energy. We will discuss these approaches and compare some of their results with the emulator presented here in Section 4. The paper is organized as follows. In Section 2 we describe the cosmological parameter space covered and provide relevant details of the simulation suite used to build the emulator. In Section 3 we discuss em-

ulator construction with a focus on error estimates. We compare our results to other approaches in Section 4, ending with a summary and outlook in Section 5. The emulator is publicly available via a github repository¹ and on our CosmicEmu webpage².

2. PARAMETER RANGES AND SIMULATIONS

The parameter range now allows for dynamic dark energy and varying the neutrino mass sum. The Mira-Titan Universe suite of simulations is well on its way to completion; we describe below the general characteristics of the simulations, including a separate discussion of how neutrinos are included.

2.1. Parameters

The choices for the parameter ranges covered in this paper are discussed in detail in Heitmann et al. (2015). In addition to the five standard parameters describing the Λ CDM model, we include a dynamical dark energy equation of state, parameterized by (w_0, w_a) , and massive neutrinos. We fix the effective number of neutrino species to be $N_{eff} = 3.04$. The dark energy equation of state is parameterized in the standard form: $w(a) = w_0 + w_a(1-a)$ (Chevalier & Polarski 2001; Linder 2003). Our parameter ranges are informed by recent observations of the CMB and large scale optical surveys. In addition, we aim to cover the relevant ranges for ongoing and upcoming surveys. With these considerations in mind, we choose the following ranges over the eight cosmological parameters (with a flat prior assumption):

$$0.12 \leq \omega_m \leq 0.155, \quad (1)$$

$$0.0215 \leq \omega_b \leq 0.0235, \quad (2)$$

$$0.7 \leq \sigma_8 \leq 0.9, \quad (3)$$

$$0.55 \leq h \leq 0.85, \quad (4)$$

$$0.85 \leq n_s \leq 1.05, \quad (5)$$

$$-1.3 \leq w_0 \leq -0.7, \quad (6)$$

$$-1.73 \leq w_a \leq 1.28, \quad (7)$$

$$0.0 \leq \omega_\nu \leq 0.01. \quad (8)$$

Note that w_a is actually jointly constrained with w_0 such that $0.3 \leq (-w_0 - w_a)^{1/4}$. See Heitmann et al. (2015) for a discussion.

2.2. Simulations

The large-scale simulations described in this paper were carried out with the HACC (Hardware/Hybrid Cosmology Code) framework, a high-performance cosmology code, designed to take advantage of current and future supercomputer architectures; HACC is described in detail in Habib et al. (2016). HACC simulations were carried out on the Mira supercomputer at the Argonne Leadership Computing Facility (ALCF) and on the Titan system at the Oak Ridge Leadership Computing Facility (OLCF). Mira belongs to the family of IBM's Blue Gene Q systems (BG/Q) and has 786,432 compute cores, while Titan achieves its high performance due to the NVIDIA K20 Graphics Processing Units (GPUs) attached to each of its $\sim 18,000$ compute nodes. The simulations described in this paper are modest in size compared to the capabilities of these machines, but the sheer number of simulations needed for our full program (~ 100) makes this work computationally expensive. We note

¹<https://github.com/lanl/CosmicEmu>

²<http://www.hep.anl.gov/cosmology/CosmicEmu/emu.html>

that HACC uses different algorithms on the above systems but the results for the power spectrum agree to within small fractions of a percent (Habib et al. 2016), much smaller than the final target error of the emulator.

The results for each sampled cosmological model were obtained as follows. We first evaluate the power spectrum using the TimeRG perturbative approach (introduced in Pietroni 2008), as described in Upadhye et al. (2014). This provides a smooth and very accurate prediction of the power spectrum on large scales (small k), out to $k \sim 0.04 \text{Mpc}^{-1}$ for $0 \leq z \leq 1$ and $k \sim 0.14 \text{Mpc}^{-1}$ for $z \leq 2$. Several N-body simulations were carried out next. In order to cover the intermediate scales (out to $k \sim 0.25 \text{Mpc}^{-1}$), we use 16 realizations of particle mesh (PM) simulations carried out with HACC. These simulations evolve 512^3 particles on a 1024^3 grid and cover a volume of $(1300 \text{Mpc})^3$ each. For the small scale (high k) regime we carry out one high-resolution simulation with HACC per cosmology. These simulations evolve 3200^3 particles starting at $z_{in} = 200$ using the Zel'dovich approximation, each in a $(2100 \text{Mpc})^3$ volume, leading to a mass resolution of approximately $\sim 10^{10} M_{\odot}$, depending on the detailed cosmological parameters. The force resolution of these simulations is $\sim 6.6 \text{kpc}$. For each of the high resolution runs we store a range of outputs:

- Particle outputs (full and randomly down-sampled to 1%) at the following redshifts: $z = \{4.00, 3.04, 2.48, 2.02, 1.78, 1.61, 1.38, 1.21, 1.01, 0.78, 0.74, 0.70, 0.66, 0.62, 0.58, 0.54, 0.50, 0.47, 0.43, 0.40, 0.36, 0.30, 0.24, 0.21, 0.15, 0.10, 0.0\}$
- Halo information at the same redshifts for friends-of-friends halos with a linking length of $b = 0.168$ with at least 20 particles per halo, halo centers are based on a potential minimum evaluation
- Halo information at eight redshifts for friends-of-friends halos with a linking length of $b = 0.2$ with at least 20 particles per halo; halo centers are based on a potential minimum evaluation
- Halo information at the same redshifts for spherical overdensity halos with M_{200} with at least 1,000 particles per halo
- Halo information at eight redshifts for spherical overdensity halos with M_{300}, M_{500} with at least 1,000 particles per halo
- All particles that reside in halos with at least 1,000 particles, 1% of particles in smaller halos, randomly selected, at least 5 particles per halo
- Particle and halo tags for all particles in halos
- Power spectra at the same redshifts, though only the following are used for building the emulator: $z = \{2.02, 1.61, 1.01, 0.66, 0.43, 0.24, 0.10, 0.0\}$

Keeping this data leads to an uncompressed dataset size of approximately 38TB per model, and more than 1PB for the simulation suite discussed in this paper. Storing the relatively large number of time slices allows for creating light-cones from the outputs, following the approach presented in Sunayama et al. (2016). For the power spectrum emulator, generation of a subset of the power spectrum measurements is sufficient due to

the smooth evolution of $P(k)$. In addition, many more emulators can be created from this data set, for quantities such as the mass function, galaxy correlation function, etc. While it is difficult to make the full dataset publicly available (the raw particle outputs will reside on tape for long-term storage and retrieval is currently slow), we are planning to make the processed data, such as the halo catalogs, publicly available in the near future.

2.2.1. Treatment of Neutrinos

The treatment of neutrino effects in cosmological simulations is nontrivial. This is mainly due to two issues: 1) the very high neutrino thermal velocities early on in the simulation, and 2) the very large mass ratio between the dark matter tracer particles and the neutrino tracer particles. Many solutions to these problems have been discussed in the literature, from adding the neutrinos only at late times, when the thermal velocities are much smaller (helping with the first but not the second problem), to introducing coarser force resolution for the neutrinos to avoid the second problem, to treating the neutrinos perturbatively (for more details, see, e.g., Agarwal & Feldman (2011); Bird et al. (2012); Brandbyge et al. (2008); Brandbyge & Hannestad (2009, 2010); Gardini et al. (1999); Inman et al. (2015); Klypin et al. (1993); Viel et al. (2010); Banerjee & Dalal (2016) and references therein).

We follow the approach discussed in detail in Heitmann et al. (2015), applying a small correction to account for the scale dependence of the growth function as discussed in Upadhye et al. (2014). We provide a short summary of our neutrino treatment here and show comparisons to results found by other groups in Section 4. Since we consider the case of relatively small neutrino masses, the most conservative treatment of neutrinos suffices. In this treatment, the neutrinos are not evolved as a separate species, but the linearly evolved neutrino component is added at each redshift separately. At $z = 0$, the simulation is normalized to the full linear neutrino-baryon-CDM power spectrum as given by CAMB (Lewis et al. 2000). The baryon-CDM component is taken to the starting redshift with a scale-independent growth function and evolved forward with the N-body code, including the neutrino component in the background equations. This is done for consistency, since the forward evolution does not have the scale-dependent growth characteristic of massive neutrinos. At each redshift of interest, we add the linear neutrino power spectrum to the nonlinear baryon-CDM component. This approach is valid as long as the neutrino density fraction $f_{\nu} \equiv \Omega_{\nu}/\Omega_m$ is sufficiently small.

The result of the procedure outlined above is a low-redshift power spectrum that accurately includes nonlinearity in the CDM + baryon sector as well as neutrinos treated linearly. Castorina et al. (2015) have found this assumption to be accurate at the 1% level for neutrino masses satisfying current bounds, when compared with N-body simulations that include massive neutrinos as separate particles. Meanwhile, at higher redshifts $z \gtrsim 1$, our use of the scale-independent CDM + baryon growth factor leads to an error at large scales where neutrinos cannot be neglected. Fortunately, these scales are linear, and Upadhye et al. (2014) showed that the resulting error can be removed by multiplying the N-body power spectrum by the k -dependent correction factor $D_{b+\text{CDM}+\nu}(k, z)^2/D_{b+\text{CDM}}(z)^2$. Here $D_{b+\text{CDM}+\nu}$ and $D_{b+\text{CDM}}$ are, respectively, the linear growth factors for baryons + CDM + ν and baryons + CDM. The corrected N-body power spectrum is consistent with perturbation theory at large scales to within the simulation error bars. This proce-

ture can be interpreted in the separate universe sense where it has been shown that the scale-dependent clustering of an extra field (quintessence or neutrinos) can be neglected (up to some level of approximation) when the simulation box size is smaller than the Jeans length of that field (Hu et al. 2016; Chiang et al. 2016). Our neutrino treatment is reasonable below the Jeans (neutrino free-streaming) scale, and we correct it on super-Jeans-scales.

3. EMULATOR CONSTRUCTION AND TESTING

In this Section we discuss the range and validity of the emulator including the possibility of adding baryonic corrections in post-processing, the smoothing procedure applied to the power spectrum from the set of individual simulations to produce the mean spectrum, and the final process of constructing the emulator. In the latter two cases we discuss the associated errors and how they are estimated and checked.

3.1. Range of Validity

Upcoming surveys require accurate predictions of the matter power spectrum at levels of a fraction of a percent. The error budget is complicated as many interacting sources of uncertainty are present. First, the numerical accuracy of the underlying cosmological simulations induces an irreducible error. We follow here the discussions in Heitmann et al. (2010) in setting the starting redshift and force and mass resolution. Given our simulation specifications, the numerical accuracy at the redshifts ($z \leq 2$) and scales ($k \leq 5\text{Mpc}^{-1}$) of interest is at the percent level. Second, there are errors due to the emulation scheme; we discuss these and estimate their values below. The main source for inaccuracy is the limited number of models that we consider here. As stated earlier, this error will reduce significantly as more models are added. Finally, the largest systematic uncertainty is due to the modeling of neutrinos and incomplete knowledge of baryonic effects.

Strictly quantifying the error of the neutrino treatment is difficult since no error-controlled, fully self-consistent, neutrino simulation exists currently. As explained in Section 2.2.1, we treat the neutrinos not as a separate species but evolve them only in the background, and we add the linear neutrino power spectrum to the P_{cb} -component obtained from the simulation rather than compute the nonlinear neutrino power spectrum. The validity of the first assumption was tested in Upadhye et al. (2014) using TimeRG perturbation theory. In the regime that the perturbative approach is valid, the agreement was excellent. The second assumption, investigated in detail in Castorina et al. (2015), holds at the 1% level.

A similar situation holds for the uncertainty due to the lack of a baryonic treatment. In our simulation, the baryons are only included in the initial transfer function and gas dynamics and star formation and feedback effects are not modeled. Baryonic effects on the power spectrum remain inconclusive due to uncertainties in the modeling of several effects, such as feedback from active galactic nuclei (AGN) and supernovae (SNe). Attaining predictive control at the percent level at smaller length scales ($k > 1\text{Mpc}^{-1}$) is difficult due to these uncertainties.

An alternative approach to carrying out a large number of expensive hydrodynamics simulations was put forward in Mead et al. (2015). Here the authors incorporate baryonic effects into a halo model approach and are able to reproduce results from full hydrodynamics simulations at the 5% level of accuracy. In the same spirit, one could model baryonic effects

given emulator predictions if reliable results from hydrodynamics simulations are available. Zentner et al. (2013) follow a similar path targeting the convergence power spectrum in modeling baryonic effects by varying the halo concentration. Approaches where the baryonic physics is modeled on top of the matter power spectrum informed by a small number of hydrodynamics simulations will be the only viable option for the foreseeable future. Eifler et al. (2015) propose using a PCA decomposition of the OWLs suite of simulations to parameterize the effect of baryons on the matter power spectrum, which can then be included in cosmological model fitting and subsequently marginalized. Kitching et al. (2014) and MacCrann et al. (2014) introduce another method to account for the impact of baryons in the dark matter power spectrum by multiplying the Halofit power spectrum by the ratio of the OWLs dark matter and baryonic power spectrum over the OWLs dark only power spectrum. Typically the most extreme OWLs simulation is chosen, the AGN feedback scenario, such that the impact of baryonic effects is maximized to provide an upper bound. This technique was applied by the Dark Energy Survey Collaboration (2016) and Kwan et al. (2017) to estimate the effect of baryonic physics on the power spectrum of cosmic shear and tangential shear for galaxy-galaxy lensing respectively.

With increasing computing power, a better understanding of uncertainties in sub-grid modeling, and more observational data for cross-calibration, the situation will likely improve over time. Given current uncertainties, it is nevertheless difficult to state an absolute error on the full matter power spectrum over the range of scales considered in this paper.

3.2. Smoothing

Our overall approach uses ideas described in the Coyote Universe series of papers (Heitmann et al. 2010, 2009; Lawrence et al. 2010; Heitmann et al. 2014). In this subsection and the next, we briefly describe the approach, referring the reader to the earlier work for further details.

The first task is to smooth the noisy power spectra generated from the N-body simulations. We use the process convolution algorithm described in Lawrence et al. (2010). A process convolution is a mechanism for producing realizations of a smooth function as a weighted average of a simple stochastic process. Figure 3 in Lawrence et al. (2010) shows a simple example with Gaussian variates (the stochastic process) averaged with a Gaussian smoothing kernel (the weighting scheme).

As in our previous work, we assume that the unobservable smooth power spectrum is the result of a two-layer process convolution. The top layer describes the transformed power spectrum as a process convolution where Brownian motion realized on a grid is smoothed with a Gaussian kernel whose kernel width changes over the domain. The kernel width is described by a the second layer process convolution which is simply Gaussian variates on a grid smoothed with a Gaussian kernel. The spectrum computed from each N-body simulation is modeled as a multivariate Gaussian variable with mean given by the two-layer process convolution and known diagonal covariance. The unknown smooth spectrum and a number of nuisance parameters are estimated using a Markov chain Monte Carlo (MCMC) based approach. Details of the procedure are provided in Lawrence et al. (2010).

The current results are obtained making a slightly different assumption compared to our previous work. Earlier we assumed, and it appeared to be the case, that different resolutions

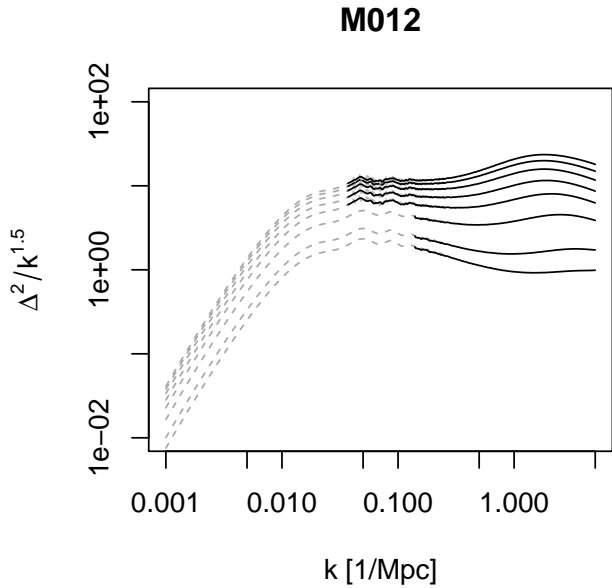


FIG. 1.— Data from the M012 run used in the process convolution estimation of the smooth spectra. The gray dashed lines show TimeRG perturbation theory results used at low k . The dotted gray lines show the low resolutions runs at medium k . The solid black line shows the high resolution run at medium and high k . In ascending order, these are at redshifts 2.020, 1.610, 1.006, 0.656, 0.434, 0.242, 0.101, and 0.000.

had about the same variance for any given value of k for which a given resolution was unbiased. It now appears that our current high resolution spectra have smaller variance about the true spectrum than the low resolution runs. For now, we have used the larger variance associated with the lower resolution runs in

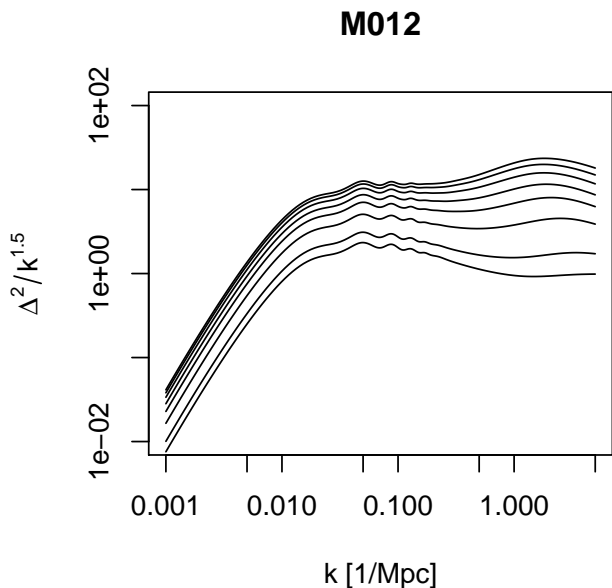


FIG. 2.— Smooth power spectra estimates for the M012 results. In ascending order, these are at redshifts 2.020, 1.610, 1.006, 0.656, 0.434, 0.242, 0.101, and 0.000.

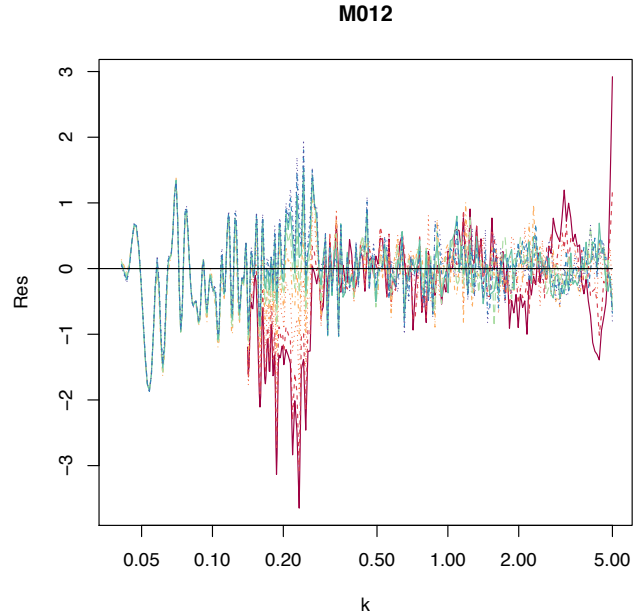


FIG. 3.— Standardized residuals from the high resolution spectra as a function of k for M012. The lines go from yellow to green to blue with increasing step (decreasing z). These show no obvious trend, suggesting that the smooth estimate is a good fit.

every case – as shown below this does not adversely affect the results. In future iterations, however, we will take this change in variance into account.

As one example, Figure 1 shows the data from the M012 runs that are used in the estimation procedure for the smooth power spectra. The dashed gray lines show the TimeRG perturbation theory results used up to $k = 0.04\text{Mpc}^{-1}$ for $z < 1$ and up to $k = 0.14\text{Mpc}^{-1}$ for $z > 1$. The gray dotted lines show the lower resolution runs that go from the TimeRG perturbation theory results up to $k = 0.25\text{Mpc}^{-1}$. The solid black line shows the high resolution run used from the TimeRG perturbation theory results up to the maximum value of $k = 5\text{Mpc}^{-1}$. Figure 2 shows the estimated smooth spectra for this simulation. M012 is representative of the results for all parameter settings (the Appendix provides a complete list of the sampling design space).

Figures 3 and 4 show some diagnostics for the process convolution fit. Both of these plots consider the standardized residuals for the high resolution run for cosmology M012 (the other cosmologies and resolutions lead to similar conclusions). The standardized residuals are computed in the following manner. First, the smoothed process convolution estimate is subtracted off across k . If the process convolution process has provided a good estimate for the mean, the residuals should now have zero mean across k , that is the mean taken across k should be close to zero. Next, each residual is divided by the standard deviation, the square root of the variance, of the raw data at each k . This variance changes over k in a log-linear fashion, i.e., the log of the variance decreases linearly with the logarithm of k . This behavior is used as part of the process convolution procedure (see Lawrence et al. 2010 for details.) If this variance prediction is correct, the resulting standardized residual should have variance one. If there is little correlation, the collection of standardized residuals should resemble an independent sample from the standard normal distribution.

TABLE 1
ADDITIONAL MODELS FOR TESTING

Model	ω_m	ω_b	σ_8	h	n_s	w_0	w_a	ω_ν
M038	0.1467	0.0227	0.7325	0.5902	0.9562	-0.8019	0.3628	0.007077
M039	0.1209	0.0223	0.8311	0.7327	0.9914	-0.7731	0.4896	0.001973
M040	0.1466	0.0229	0.8044	0.8015	0.9376	-0.9561	-0.0359	0.000893
M041	0.1274	0.0218	0.7386	0.6752	0.9707	-1.2903	1.0416	0.003045
M042	0.1244	0.0230	0.7731	0.6159	0.8588	-0.9043	0.8095	0.009194
M043	0.1508	0.0233	0.7130	0.8259	0.9676	-1.0551	0.3926	0.009998
M044	0.1389	0.0224	0.8758	0.6801	0.9976	-0.8861	-0.1804	0.008018

Figure 3 presents evidence that the process convolution works well in capturing the mean structure. The residuals are centered on zero across k and there are no major trends in the data, supporting the unbiased nature of the mean estimate. (There is some evidence of oscillatory behavior at high k , which might indicate that our process convolution mean is not flexible enough or might arise for some other cause; either way, it is not quantitatively significant.) Here we see some confirmation of the aforementioned fact that the high resolution runs have smaller variance than the low resolution run. Most of these residuals are between -1 and 1, which is too small to match our assumption that these residuals should resemble draws from a standard normal (which would produce numbers mostly between -3 and 3). Figure 4 tests our distribution of Gaussianity. Here, the empirical quantiles of the standardized residuals (basically the sorted residuals) are plotted against the theoretical quantiles of the standard normal distribution. The colors match Figure 3. The straight lines indicate that the residuals do appear to be Gaussian and are relatively uncorrelated. The slope of the lines is related to the variance. The fact that these are less than unity is another indication that the variance of these residuals is smaller than expected. This conclusion about the variance is not detrimental as every indication is that we are estimating the smooth spectra well and the errors are fairly Gaussian.

3.3. Emulation

The follow-on task is to construct the emulator from smooth estimates of the matter power spectra. As in the extension of the original Cosmic Emulator in Heitmann et al. (2014), we also have a number of partial power spectra using the TimeRG perturbation theory approach. In fact, we have results from TimeRG perturbation theory for the complete design (111 models). To build the emulator, we follow a version of the basic plan from Heitmann et al. (2014). Our goal is to predict the multivariate power spectrum from an N-body simulation as a function of the eight input parameters. As detailed in Lawrence et al. (2010), the first step is to standardize the simulation outputs by centering and scaling, and then projecting them on to an empirical basis computed via SVD (i.e., principal components or empirical orthogonal functions). This process discovers the directions of greatest variation in the high-dimensional outputs and reduces the modeling to these dimensions. The basis weights are then modeled as functions of the simulation inputs using Gaussian processes.

In this case, we have TimeRG perturbation theory results for the entire 111 run design and complete, smoothed spectra from N-body results over the first 36 runs in the design. The 36 complete runs are used to compute the mean vector, the scaling fac-

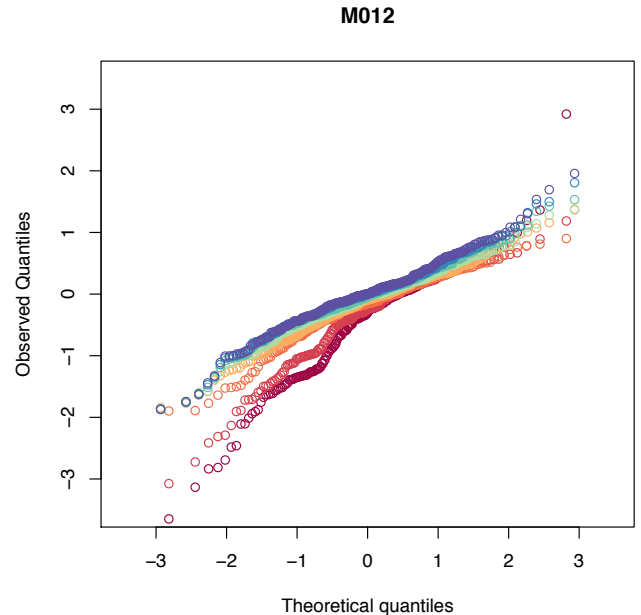


FIG. 4.— Quantile-quantile plot for the standardized residuals from the high resolution spectra for M012. The points go from yellow to green to blue with decreasing redshift z . Empirical quantiles are plotted against the theoretical quantiles of the standard normal distribution. The approximately straight lines indicate that the sample is close to normal. The slope suggests that the variance is somewhat smaller than expected, as discussed in the text.

tor, and 35 basis vectors. The complete spectra are centered, scaled, and projected onto the basis to obtain their weights. The partial TimeRG perturbation theory power spectra (up to the k values described in the description of the smoothing) are centered using the relevant portion of the mean vectors, scaled, and then projected on to the relevant part of the basis vectors to obtain their weights. However, the partial power spectra are only projected onto the first 7 basis vectors. This number was chosen by comparing the weights from the partial and complete runs. Beyond 7 basis vectors, the weights from the partial runs begin to differ visually from the weights from the complete runs when plotted against the eight input parameters. As a result, using the partial run weights will actually begin to degrade the performance of the emulator. All of the weights, from both complete and partial spectra are put together to estimate the Gaussian process emulator. See Lawrence et al. (2010); Heitmann et al. (2014) for details on the estimation via an MCMC based approach.

Figure 5 shows test results of the emulator fit for the total matter power spectrum emulator, $P_{tot} = (P_{cb}^2 + P_{\nu}^2)^{1/2}$. The dashed lines show the results for spectra from design points M038-M044, which are completed runs from the next stage of the emulator lattice design. The tests are done by holding out the partial TimeRG perturbation theory results for these runs and predicting the complete spectra. The maximum error is about 3% and most are below 2%. The solid lines are the results for the best fit cosmology M000. This is a true out of sample test. At low k the error reaches its maximum, with one redshift showing about a 2.5% error. Figure 6 shows the results from predicting the training set. Typically, emulators are expected to interpolate the training set, but that is not true in the current case. It seems likely that the emulator has difficulty interpolating the weights from the TimeRG perturbation theory-only results. The resulting fit becomes more like standard regression where the data is not interpolated, but errors are minimized. This issue shows up most prominently at high k where the TimeRG perturbation theory-only runs provide no direct information. Still, the worst-case error is only 5% with the vast majority of errors under 2%. (These numbers are consistent with the linear theory tests carried out in Heitmann et al. 2015.) As the number of complete runs continues to increase in later releases, we anticipate that this issue will disappear; tests using the linear theory results from Heitmann et al. (2015) are consistent with this expectation. Overall, the emulator performs very well despite only 36 complete sets of spectra in eight dimensions. We also measured the errors in just the the baryon-dark-matter component, $P_{cb}(k)$, finding very similar results.

4. COMPARISON WITH OTHER APPROACHES

In this section we provide some comparisons with alternative approximate prediction methods. Since most other groups have addressed either neutrinos or a dynamical dark energy equation of state but not both (as done here), we divide our tests accordingly. In each of the following subsections we compare the alternative approaches to our full simulations, if an appropriate model is available. In addition, we use a set of new models that

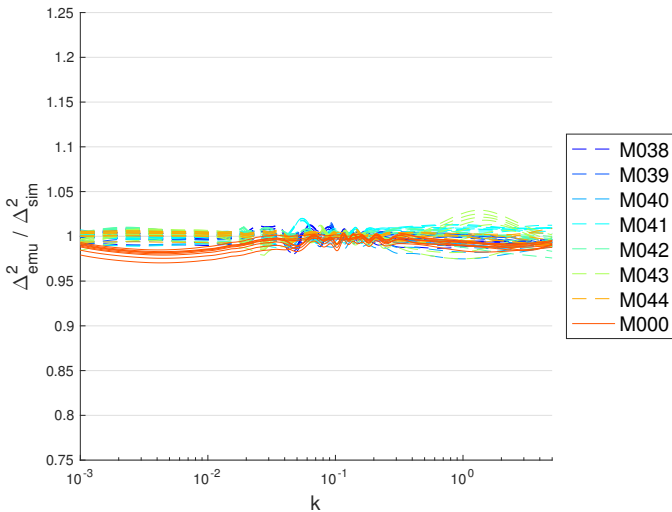


FIG. 5.— Total matter power spectrum predictions for the cosmologies M038-M044 (completed runs from the next design stage, not used in the current work) and the best fit WMAP7 cosmology M000. The former are a hybrid of out-of-sample and cross-validation predictions as the TimeRG perturbation theory-only runs for these cosmologies were held-out on each prediction. The model, M000, is a true test set. The comparison implies that the error is less than 3%.

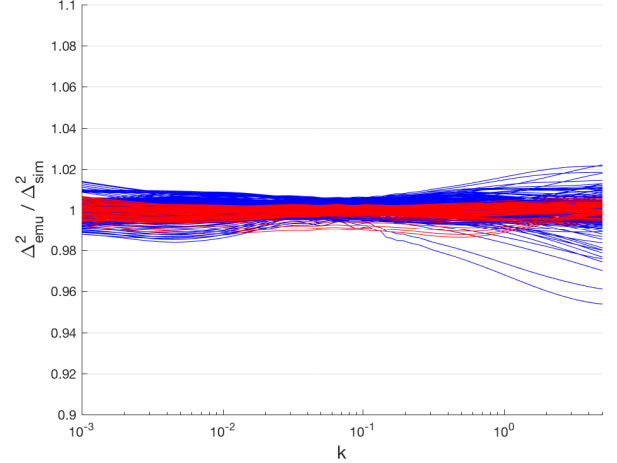


FIG. 6.— Total matter power spectrum predictions for the training set. Red lines show simulations with $\omega_{\nu} = 0$ (M000-M010) while blue lines show simulations with non-zero neutrino masses (M011-M036). Normally, an emulator is expected to interpolate these exactly, but the inclusion of weights from the partial runs makes this difficult. The resulting emulator behaves somewhat more like standard regression which does not interpolate, but minimizes error. These results suggest that the error may be as high as 5% in some cases. As the number of runs increases, this issue will be resolved (see text).

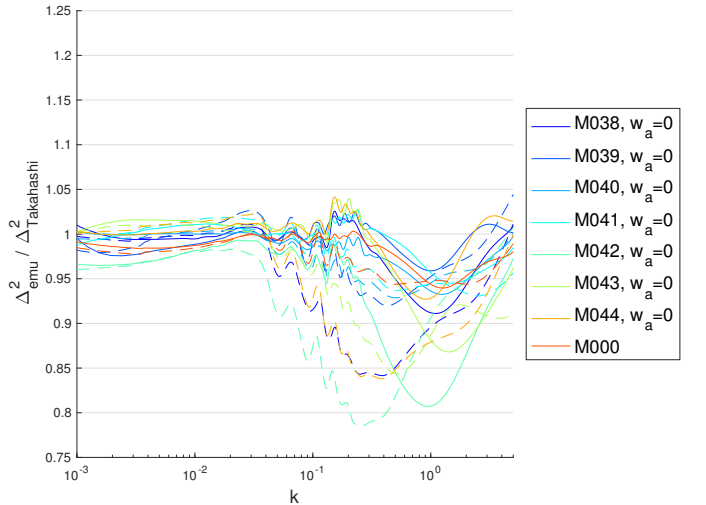


FIG. 7.— Ratio of predictions from the new emulator with those obtained using the method of Takahashi et al. (2012). Solid lines show results at $z = 2.02$ while dashed lines show results at $z = 0$. The methods match very well at low k (at the 2-3% level), but differ by 20% at high k for the higher neutrino masses with $\omega_{\nu} > 0.007$ (M038, M042, M043, M044). For the models with $\omega_{\nu} < 0.031$, the agreement is better than 7% over most of the k -range investigated.

are not in the simulation design to compare the emulator with the other prediction schemes if those schemes do allow variation of all eight parameters. We carry out our comparisons for the two extreme redshifts, $z = 0$ and $z = 2.02$.

4.1. Neutrino Predictions

For the case of power spectrum predictions including neutrinos, we study the Halofit approach by Takahashi et al. (2012), which was augmented with a neutrino term by Bird et al. (2012). Takahashi et al. (2012) improved the Halofit model originally developed by Smith et al. (2003) around the Λ CDM model by adding a set of sixteen high-quality gravity-only simulations. Six of those models were chosen around the best-

fit WMAP results from different years. The other ten were at the same design points as the first ten models from the original Coyote Emulator (Lawrence et al. 2010) (the simulation results agreed with those run for the Coyote Emulator mostly within 3%). These additional simulations allowed them to include a constant equation of state parameter w as a new cosmological parameter. Next, they refitted their parametric model (adding additional parameters) to achieve an accuracy at the 5-10% level out to $k \leq 10h\text{Mpc}^{-1}$. Based on this work, Bird et al. (2012) added a neutrino component to Halofit with a new set of simulations covering neutrino masses between $0.15 \leq \sum m_\nu \leq 0.6\text{eV}$. Their neutrino treatment is particle-based, with the neutrinos modeled as a separate species, albeit at lower force resolution than the dark matter particles. In order to avoid problems due to large neutrino velocities, they started the simulations as late as $z_{\text{in}} = 24$ for the lightest neutrinos, using the Zel'dovich approximation. This leads to systematic inaccuracies in the power spectrum at the few percent level as shown in Heitmann et al. (2010) and Schneider et al. (2016). (In both papers effects at the 2-3% level were shown with a starting redshift $z_{\text{in}} = 50$ at $k \sim 1h\text{Mpc}^{-1}$, extrapolating these results would suggest a 5% error due to the late start alone, and even more at higher k). In addition, the small volumes and limited mass resolution (512^3 particles) further degrade the accuracy of the simulations. All these effects combined will lead to systematic errors and scatter in the power spectrum, in particular on small length scales. The neutrino-augmented results are available in the latest CAMB release and have been updated over time (Lewis et al. 2000).

Figure 7 shows a comparison of our new emulator with the Takahashi et al. (2012) implementation. The ΛCDM model (M000, brown line) agrees with our emulator at the 5% level at $z = 0$ which is in agreement with our previous findings in Heitmann et al. (2014) for the same model (see Fig. 11 in that paper. Note that in the extended emulator paper the ratio is taken with respect to the simulation, meaning that the y -axis in that paper is the inverse from what we show in Figure 7 here). Our finding of very similar agreement with Takahashi et al. (2012) with the new emulator for M000 stresses the excellent agreement between GADGET-2 and HACC (the original Coyote Emulator papers were based on GADGET-2 simulations, while the new simulations have been carried out with HACC, agreements are well within the sub-percent level). Similar results comparing GADGET-2 and HACC were also reported in the HACC code paper by Habib et al. (2016).

For all models, the agreement on large scales (small k , $k < 0.02\text{Mpc}^{-1}$) is at the 1-2% level at both redshifts, $z = 0$ and $z = 2.02$, demonstrating that our use of a k -dependent correction factor for the growth function works very well. In the quasilinear to nonlinear regime the agreement between the Halofit approach and the new emulator varies between 5% up to 20%. This is again consistent with our previous findings in Heitmann et al. (2014), Figure 12, where for some cosmological models, the differences for the power spectrum prediction between Halofit and the extended emulator were as large as 15% over a similar k -range ($0.1\text{Mpc}^{-1} < k < 1\text{Mpc}^{-1}$). Contemplating this level of error in Halofit is discomfoting in the context of using the matter power spectrum to obtain cosmological constraints, since these deviations of around $\sim 10 - 15\%$ occur in the range of scales typically accessed by measurements of the cosmic shear power spectrum.

Finally, we emphasize that as shown in our previous work by Upadhye et al. (2014), the agreement of our simulations in-

cluding neutrinos with a TimeRG-based perturbative approach was better than 2% at $\sim 0.2\text{Mpc}^{-1}$ at $z = 2$ and $\sim 0.1\text{Mpc}^{-1}$ at $z = 0$, for values of ω_ν as high as 0.01. Given these results, in combination with the findings in Castorina et al. (2015) discussed in Section 2.2.1, the differences in Halofit and the new emulator are apparently due to the general inaccuracy of Halofit away from ΛCDM models rather than to the different neutrino treatment applied.

4.2. Dynamical Dark Energy Equation of State Predictions

Next we compare our results with the work of Casarini et al. (2016). Based on our earlier emulator work in Heitmann et al. (2014), these authors developed a prediction for (w_0, w_a) cosmologies by introducing an effective constant equation of state that captures the influence of a time-varying dark energy equation of state to sub-percent accuracy. This idea was introduced in Francis, Lewis, & Linder (2007) and is based on the assumption that cosmologies beyond ΛCDM can be mapped back to $w\text{CDM}$ models by requiring both models to have the same distance to last scattering and the same values of H_0 and energy densities, $\Omega_{m,r,b,0}$ at $z = 0$. This has the effect of tuning the growth in constant w_0 models to match the (w_0, w_a) models of interest for some new value of σ_8 . The new value of σ_8 is constrained by the chosen values of (w_0, w_a) and within the context of the Coyote emulator, this limits the space of allowable models because of the parameter range of the design.

Based on the above general idea and the results from Heitmann et al. (2014) for $w\text{CDM}$ models, Casarini et al. (2016) deliver predictions for the nonlinear power spectrum for dynamical dark energy models for scales of $1 < k < 1.5$ and between redshift $0 \leq z \leq 3$ at high accuracy.

Before we show a comparison of the Casarini et al. (2016) approach with the emulator, we compare two of our smoothed power spectra from the simulations for M005 and M007 directly with their prediction in Figure 8. By testing against the smoothed input power spectra as well, we are able to distinguish between various sources of error in Figure 8, that is, whether the discrepancy, should there be any, is due to the as-

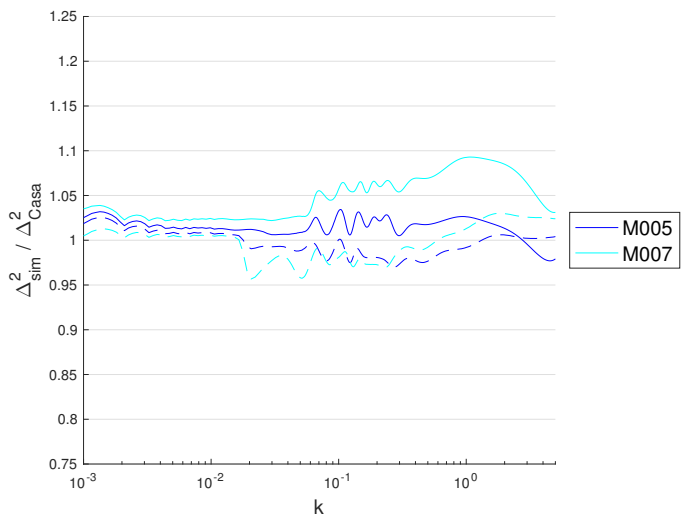


FIG. 8.— Ratio of simulation results with those obtained using the method of Casarini et al. (2016) for M005 and M007. We compare at $z = 2$ (solid line) and $z = 0$ (dashed line). For M007 we have $w_a = -1.0$ and for M008 we have $w_a = 0.4333$. The values for ω_m and σ_8 are higher for M007, leading to stronger nonlinear effects. The Casarini et al. (2016) approach leads to $< 5\%$ inaccuracy for M005 and $< 10\%$ for M007.

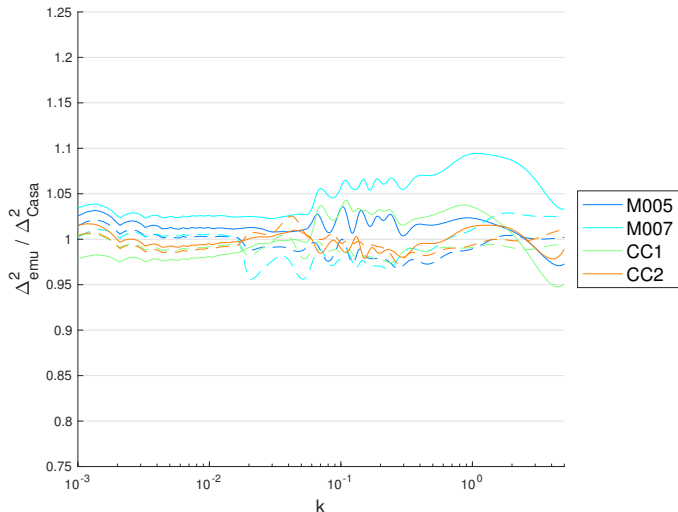


FIG. 9.— Ratio of predictions from the new emulator with those obtained using the method of Casarini et al. (2016). CC1 and CC2 are cosmologies selected in addition to M005 and M007 for this comparison. The inputs are $\omega_m = 0.14205$, $\omega_b = 0.02225$, $\sigma_8 = 0.83$, $h = 0.6727$, $n_s = 0.9645$ and $\omega_\nu = 0$ for both CC runs. For CC1, we choose $w_0 = -1.0$ and $w_a = 0.5$ and for CC2, $w_0 = -1.0$ and $w_a = -0.5$. For all cosmologies, we compare at $z = 2$ (solid line) and $z = 0$ (dashed line). The methods match reasonably well, agreeing within 10% errors. The disagreement between the emulator and the Casarini et al. (2016) result for M005 and M007 is at the same level as the disagreement of direct comparison with the simulations in Figure 8, consistent with our emulator test shown in Figure 6.

assumptions of the Casarini et al. model or the predictive power of the Gaussian Process modeling. The solid line shows results at $z = 2$ while the dashed lines show results at $z = 0$. The results for $z = 0$ are in agreement at a level better than 5%, for M005 at both redshifts. For M007 at $z = 0$ the agreement is also excellent (below 5%), for $z = 2$ it degrades slightly but stays well under 10%. Next, Figure 9 shows a comparison of the emulator with Casarini et al. (2016) for the same models and two additional models, CC1 and CC2 that were not part of our original design (the cosmological parameters for CC1 and CC2 are listed in the figure caption). We have chosen to include these entirely new models in our analysis because the behavior of $\sigma_8(z)$ cannot be chosen independently of the other cosmological parameters. This meant that we could only generate predictions for two models in our testing set, without massive neutrinos, staying within the Casarini et al. framework

Again, the comparisons are carried out at $z = 0$ and $z = 2$. At large scales ($k < 0.02 \text{Mpc}^{-1}$) the agreement is excellent, at the 1-2% level. In the quasi-linear to nonlinear regime, the agreement of the emulator and Casarini et al. (2016) is very similar to the agreement with respect to the simulations themselves, better than 5% for all models at $z = 0$ and well below 10% for all models at $z = 2$. This level of agreement shows that this approach works quite well.

4.3. Eight-Parameter Model Predictions

In their work, Mead et al. (2016) provide new power spectrum predictions, covering not only neutrinos but also dynamical dark energy and modified gravity models. Their approach is based on re-deriving the different contributions to the halo model. The new prediction scheme is supposed to be valid for $k < 10h \text{Mpc}^{-1}$ at the few percent level accuracy for most models. They arrive at this conclusion by comparing their results to a range of simulations. This is the only approach for which

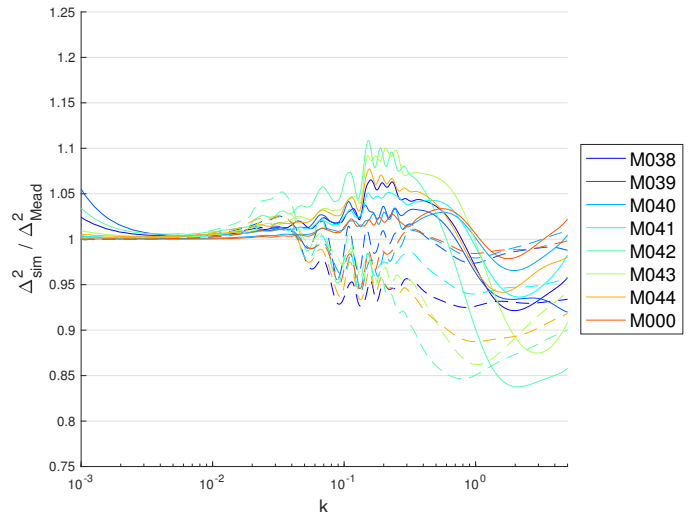


FIG. 10.— Ratio of predictions from our smoothed simulation results with those obtained using the method of Mead et al. (2016) for M038-M044 given in Table 1 and M000, our Λ CDM cosmology. As in previous plots, dashed lines show the results at $z = 0$ and solid lines at $z = 2.02$. The agreement for M000 is basically perfect on large scales and at the 2% level in the nonlinear regime. For M038-M044 the agreement is good over most of the k -range (at the 5-10% level) but discrepancies can be as large as 15%.

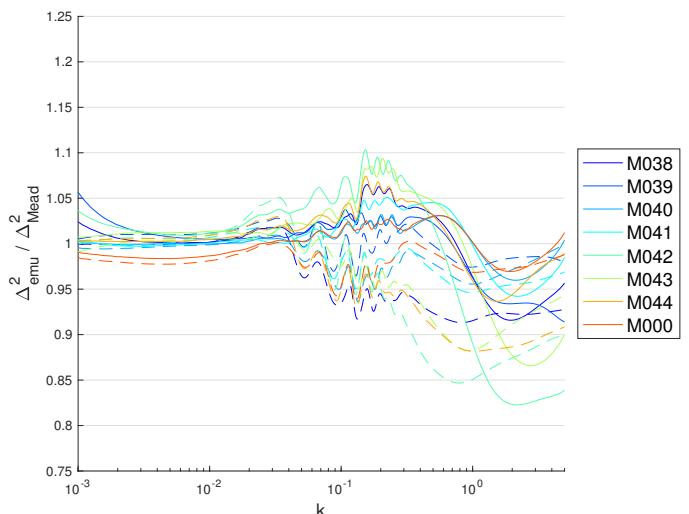


FIG. 11.— Ratio of predictions from the new emulator with those obtained using the method of Mead et al. (2016) for the same models shown in Fig. 10. The methods match roughly at the 3% level at low k for most models, but differ by more than 15% at high k consistent with the comparison to the simulations themselves shown in Figure 10.

we can compare our full emulator and our simulation results directly. We use the additional seven models for this comparison that were also employed to investigate the accuracy of our emulator, as given in Table 1.

We show the comparison of the Mead et al. (2016) fit with our smoothed simulations directly in Figure 10 for M000 and M038-M044, given in Table 1. The agreement for the Λ CDM cosmology is excellent, basically perfect on large scales up to $k \sim 0.04 \text{Mpc}^{-1}$ and at the 2–3% in the nonlinear regime. The models with a varying dark energy equation of state show some disagreement on the very largest scales, which is most likely due to our different implementation of (w_0, w_a) cosmologies in CAMB than in the version that was used by Mead et al. (2016). For relevant details the reader is referred to our previous work (Upadhye et al. 2014) where we provide a description of our

implementation and a publicly available CAMB version. In the quasi-linear regime, the agreement is around 5-10% while at $k \sim 1\text{Mpc}^{-1}$ some models show differences of up to 15%.

Figure 11 shows the ratio of the new emulator with respect to the Mead et al. (2016) fit for the same models. The results are very similar to the comparison to the smoothed simulations as to be expected from Fig. 5 (obviously, taking the ratio of Figures 10 and 11 would lead back to the results of Figure 5). On large scales, we see slightly poorer agreement compared to the comparison to the smoothed simulations, but still at the 2% level. On small scales, the agreement is very similar to the direct comparison with the simulations – for some models around 5% while for others closer to 15%.

4.4. Comparison with the Extended Emulator

Finally, as a last check, we compare our earlier, ‘Coyote Extended’ emulator, developed in Heitmann et al. (2014) with our new emulator, keeping $w_a = \omega_\nu = 0$. We list the models used for this test in Table 2. Several of the values used are close to the edge of our parameter design, making this test rather stringent. Figure 12 shows the ratio of the new emulator over the extended emulator from our previous work. We show results for eight models at redshift $z = 0$. The agreement for most models is at 2% with two instances showing disagreement up to 4%. Given the estimated accuracy of our current emulator at approximately 4% and of the previous emulator at the $\sim 5\%$ level this agreement is within the expected limits.

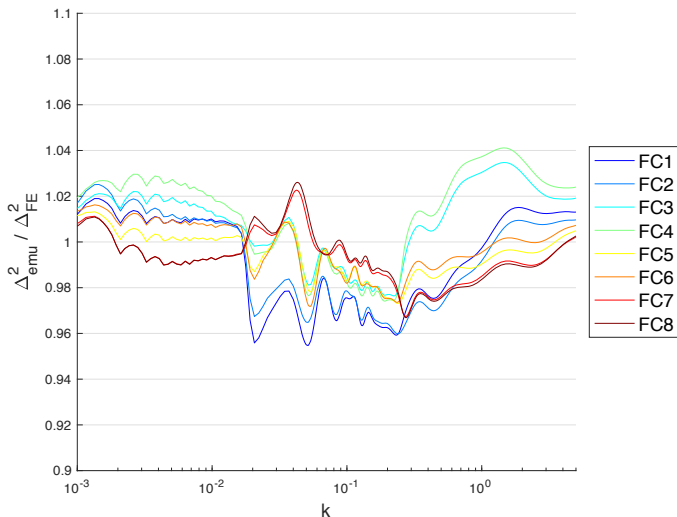


FIG. 12.— Ratio of predictions from the new emulator with those obtained using the extended Cosmic Emulator (Heitmann et al. 2014). The cosmological parameters for this comparison are given in Table 2. For all cosmologies, we compare at $z = 0$. The methods match within their separately estimated errors, with disagreements at most at 4%.

5. SUMMARY AND OUTLOOK

We introduce a new cosmic emulator for the matter power spectrum that covers eight cosmological parameters, and spans a redshift range from $0 \leq z \leq 2$ and wave numbers out to $k \sim 5\text{Mpc}^{-1}$. We achieve an accuracy at the 4% level (better for most models) over the full k -range and all eight parameters while using a sampling space of just 36 cosmological models.

The parameter sampling approach for designing the simulation suite is described in in Heitmann et al. (2015). Because this scheme has demonstrated convergence properties, the accuracy

of the emulator can be systematically improved by adding more simulations at well-defined points reaching close to 1% with about 100 evaluation points in the eight-dimensional space; the next set of 26 simulations is currently being analyzed. The internal accuracy tests presented in this paper are consistent with the estimates from the linear theory-based test presented in Heitmann et al. (2015) and with the error estimates of a previously constructed emulator that relied on a different set of simulations (Heitmann et al. 2014). These positive results are an important consistency check for our planned further improvement of the error bounds.

We have compared our results to other predictions for the nonlinear power spectrum by a number of authors. The agreement in the linear regime is excellent as is to be expected. The agreement degrades for models away from ΛCDM in the quasi-linear to nonlinear regime and we find differences at the 5–10% for most models but up to 15–20% depending on the model and redshift investigated and prediction scheme used (only Mead et al. 2016 provide predictions over the eight cosmological parameters that we investigate here, all other approaches only treat a subset of the parameters). The agreement we find between different methods is consistent with our evaluation in the extended Coyote emulator, presented in Heitmann et al. (2014), where we found differences between the emulator predictions and, e.g., Halofit at the 20% level for some models.

The simulation suite presented here lends itself to many more investigations. We are currently building a large set of emulators for quantities such as the halo mass function, redshift space distortions, and halo correlation and galaxy correlation functions and bias functions. As emulation accuracies continue to improve, addition of ‘post-processing’ modules for, e.g., baryonic effects and galaxy modeling, will also become easier to implement in a robust fashion.

In future, we expect emulators and observations to co-evolve. There will likely be a greater emphasis on cross-correlation-based probes; also as measurements squeeze the parameter space priors, the quality of emulation will improve significantly.

We thank Alexander Mead and Tim Eifler for many useful conversations. KH and SH thank the Aspen Center for Physics, which is supported by National Science Foundation grant PHY-1066293, where part of this work was carried out.

Part of this research was supported by the DOE under contract W-7405-ENG-36. Argonne National Laboratory’s work was supported under the U.S. Department of Energy contract DE-AC02-06CH11357. Partial support for HACC development and for this work was provided by the Scientific Discovery through Advanced Computing (SciDAC) program funded by the U.S. Department of Energy, Office of Science, jointly by Advanced Scientific Computing Research and High Energy Physics.

This research used resources of the ALCF, which is supported by DOE/SC under contract DE-AC02-06CH11357 and of the Oak Ridge Leadership Computing Facility at the Oak Ridge National Laboratory, which is supported by the Office of Science of the U.S. Department of Energy under Contract No. DE-AC05-00OR22725.

APPENDIX

In this Appendix we list all the cosmological models that have been used in the paper to construct and test the new emulator.

TABLE 2
EXTENDED COSMIC EMU COMPARISON COSMOLOGIES

Model	ω_m	ω_b	σ_8	h	n_s	w_0	w_a	ω_ν
FC1	0.15110	0.02217	0.81110	0.8167	1.0280	-1.09038	0	0
FC2	0.15110	0.02217	0.82813	0.8167	1.0280	-1.19484	0	0
FC3	0.12000	0.02306	0.70000	0.6833	1.0060	-0.74838	0	0
FC4	0.12000	0.02306	0.68981	0.6833	1.0060	-0.71040	0	0
FC5	0.14205	0.02225	0.83000	0.6727	0.9645	-0.84095	0	0
FC6	0.14205	0.02225	0.81830	0.6727	0.9645	-0.78951	0	0
FC7	0.14205	0.02225	0.83000	0.6727	0.9645	-1.12210	0	0
FC8	0.14205	0.02225	0.83757	0.6727	0.9645	-1.18190	0	0

TABLE 3
DESIGN

Model	ω_m	ω_b	σ_8	h	n_s	w_0	w_a	ω_ν
M000	0.1335	0.02258	0.8	0.71	0.963	-1.0	0.0	0.0
M001	0.1472	0.02261	0.8778	0.6167	0.9611	-0.7000	0.67220	0.0
M002	0.1356	0.02328	0.8556	0.7500	1.0500	-1.0330	0.91110	0.0
M003	0.1550	0.02194	0.9000	0.7167	0.8944	-1.1000	-0.28330	0.0
M004	0.1239	0.02283	0.7889	0.5833	0.8722	-1.1670	1.15000	0.0
M005	0.1433	0.02350	0.7667	0.8500	0.9833	-1.2330	-0.04445	0.0
M006	0.1317	0.02150	0.8333	0.5500	0.9167	-0.7667	0.19440	0.0
M007	0.1511	0.02217	0.8111	0.8167	1.0280	-0.8333	-1.00000	0.0
M008	0.1200	0.02306	0.7000	0.6833	1.0060	-0.9000	0.43330	0.0
M009	0.1394	0.02172	0.7444	0.6500	0.8500	-0.9667	-0.76110	0.0
M010	0.1278	0.02239	0.7222	0.7833	0.9389	-1.3000	-0.52220	0.0
M011	0.1227	0.0220	0.7151	0.5827	0.9357	-1.0821	1.0646	0.000345
M012	0.1241	0.0224	0.7472	0.8315	0.8865	-1.2325	-0.7646	0.001204
M013	0.1534	0.0232	0.8098	0.7398	0.8706	-1.2993	1.2236	0.003770
M014	0.1215	0.0215	0.8742	0.5894	1.0151	-0.7281	-0.2088	0.001752
M015	0.1250	0.0224	0.8881	0.6840	0.8638	-1.0134	0.0415	0.002789
M016	0.1499	0.0223	0.7959	0.6452	1.0219	-1.0139	0.9434	0.002734
M017	0.1206	0.0215	0.7332	0.7370	1.0377	-0.9472	-0.9897	0.000168
M018	0.1544	0.0217	0.7982	0.6489	0.9026	-0.7091	0.6409	0.006419
M019	0.1256	0.0222	0.8547	0.8251	1.0265	-0.9813	-0.3393	0.004673
M020	0.1514	0.0225	0.7561	0.6827	0.9913	-1.0101	-0.7778	0.009777
M021	0.1472	0.0221	0.8475	0.6583	0.9613	-0.9111	-1.5470	0.000672
M022	0.1384	0.0231	0.8328	0.8234	0.9739	-0.9312	0.5939	0.008239
M023	0.1334	0.0225	0.7113	0.7352	0.9851	-0.8971	0.3247	0.003733
M024	0.1508	0.0229	0.7002	0.7935	0.8685	-1.0322	1.0220	0.003063
M025	0.1203	0.0230	0.8773	0.6240	0.9279	-0.8282	-1.5005	0.007024
M026	0.1224	0.0222	0.7785	0.7377	0.8618	-0.7463	0.3647	0.002082
M027	0.1229	0.0234	0.8976	0.8222	0.9698	-1.0853	0.8683	0.002902
M028	0.1229	0.0231	0.8257	0.6109	0.9885	-0.9311	0.8693	0.009086
M029	0.1274	0.0228	0.8999	0.8259	0.8505	-0.7805	0.5688	0.006588
M030	0.1404	0.0222	0.8232	0.6852	0.8679	-0.8594	-0.4637	0.008126
M031	0.1386	0.0229	0.7693	0.6684	1.0478	-1.2670	1.2536	0.006502
M032	0.1369	0.0215	0.8812	0.8019	1.0005	-0.7282	-1.6927	0.000905
M033	0.1286	0.0230	0.7005	0.6752	1.0492	-0.7119	-0.8184	0.007968
M034	0.1354	0.0216	0.7018	0.5970	0.8791	-0.8252	-1.1148	0.003620
M035	0.1359	0.0228	0.8210	0.6815	0.9872	-1.1642	-0.1801	0.004440
M036	0.1390	0.0220	0.8631	0.6477	0.8985	-0.8632	0.8285	0.001082

REFERENCES

- Ade, P.A.R. et al. (Planck Collaboration), 2016, *Astron. & Astrophys.* 594, A13
- Agarwal, S. & Feldman, H., 2011, *Mon. Not. Roy. Astron. Soc.* 410, 1647
- Agarwal, S., Abdalla, F.B., Feldman, H.A., Lahav, O., & Thomas, S.A., 2014, *Mon. Not. Roy. Astron. Soc.* 439, 2102
- Anderson, L. et al., 2014, *Mon. Not. Roy. Astron. Soc.* 441, 24
- Bergner, S., 2011, *Making choices in multi-dimensional parameter spaces, PhD thesis*, Simon Fraser University
- Bird, S., Viel, M., & Haehnelt, M.G., 2012, *Mon. Not. Roy. Astron. Soc.* 420, 2551
- Brandbyge, J., Hannestad, S., Haugbolle, T., & Thomsen, B., 2008, *JCAP* 0808, 020
- Brandbyge, J. & Hannestad, S., 2009, *JCAP* 0905, 002
- Brandbyge, J. & Hannestad, S., 2010, *JCAP* 1001, 021
- Banerjee, A. & Dalal, N., 2016, *JCAP* 1611, 015
- Caldwell, R. & Kamionkowski, 2009, *Ann. Rev. Nuc. Part. Sci.* 59, 397
- Casarini, L., Bonometto, S. A., Tessarotto, E., & Corasaniti, P.-S., 2016, arXiv:1601.07230
- Castorina, E., Carbone, C., Bel, J., Sefusatti, E., & Dolag, K 2015, *JCAP* 1507, 043
- Chevalier, M. & Polarski, D. 2001, *Int. J. Mod. Phys. D* 10, 213
- Chiang, C.T., Li, Y., Hu, W., & LoVerde, M., 2016, *Phys. Rev. D* 94, 123502
- The Dark Energy Survey Collaboration et al., 2016, *Phys. Rev. D*, 94, 022001
- Eifler, T., Krause, E., Dodelson, S., Zentner, A.R., Hearin, A.P. & Gnedin, N.Y., 2015, *MNRAS*, 454, 2451
- Feng, J.L., 2010, *Ann. Rev. Astron. Astrophys.* 48, 495
- Francis, M.J., G.F. Lewis, G.F., & Linder, E.V., 2007, *Mon. Not. Roy. Astron. Soc.* 380, 1079
- Gardini, A., Bonometto, S.A., & Murante, G., 1999, *ApJ* 524, 510
- Habib, S., Heitmann, K., Higdon, D., Nakhleh, C., & Williams, B., 2007, *Phys. Rev. D* 76, 083503
- Habib, S., Pope, A., Finkel, H., Frontiere, N., Heitmann, K., Daniel, D., Fasel, P., Morozov, V., Zagaris, G., Peterka, T., Vishwanath, V., Lukić, Z., Sehrish, S., & Liao, W.-k., 2016, *New Astronomy*, 42, 49
- Heitmann, K., Higdon, D., Nakhleh, C., & Habib, S., 2006, *ApJ* 646, L1
- Heitmann K., Higdon D., White M., Habib S., Williams, B.J., & Wagner, C., 2009, *ApJ* 705, 156
- Heitmann K., White M., Wagner C., Habib S., Higdon D., 2010 *ApJ* 715, 104
- Heitmann K., Lawrence, E., Kwan, J., Habib, S., & Higdon, D., 2014 *ApJ* 780, 111
- Heitmann, K., Bingham, D., Lawrence E., Bergner, S., et al., 2016, *ApJ* 820, 108
- Hu, W., Chiang, C.T., Li, Y., & LoVerde, M., 2016, *Phys. Rev. D* 94, 023002
- Inman, D., Emberson, J. D., Pen, U.-L., Farchi, A., Yu, H.-R., & Harnois-D'Avraps, J., 2015, *Phys. Rev. D* 92, 023502
- Joyce, A., Jain, B., Khoury, J., & Trodden, M., 2015, *Phys. Rep.*, 568, 1
- Klypin, A., Holtzman, J., Primack, J., & Regos, E., 1993, *ApJ* 416, 1
- Kitching, T., Heavens, A. F., Alsing, J., Erben, T., Heymans, C., Hildebrandt, H., Hoekstra, H., Jaffe, A. et al., 2014, *MNRAS*, 442, 1326
- Kwan, J., Bhattacharya, S., Heitmann, K., & Habib, S. 2013, *ApJ* 768, 123
- Kwan, J., Heitmann, K., Habib, S., Padmanabhan, N., Finkel, H., Frontiere, N. & Pope, A., 2015, *ApJ* 810, 35
- Kwan, J., Sanchez, C., Clampitt, J., Blazek, J., Croce, M., Jain, B., Amara, A., Becker .M. R. et al., 2017, *MNRAS*, 464, 4045
- Lawrence, E., Heitmann, K., White, M., Higdon, D., Wagner, C., Habib, S., & Williams, B. 2010 *ApJ* 713, 1322
- Lewis, A., Challinor, A., & Lasenby, A. 2000, *ApJ* 538, 473
- Linder, E. 2003, *Phys. Rev. Lett.* 90, 091301
- MacCrann, N., Zuntz, J, Bridle, S, Jain, B, & Becker, M.R., 2015, *MNRAS*, 451, 2877
- Mead, A.J., Peacock, J.A., Heymans, C., Joudaki, S., & Heavens, A., 2015, *Mon. Not. Roy. Astron. Soc.* 454, 1958
- Mead, A.J., Heymans, C., Lombriser, L., Peacock, J.A., Steele, O.I., & Winther, H.A., 2016, *Mon. Not. Roy. Astron. Soc.* 459, 1468
- O'Shea B.W., Bryan G., Bordner J., Norman M.L., Abel T., Harkness R., Kritsuk A., 2010, *Astrophysics Source Code Library*, 10072
- Pietroni, M. 2008, *JCAP* 10, 036
- Schneider, A., Teyssier, R., Potter, D., Stadel, J., Onions, J., Reed, D.S., Smith, R.E., Springel, V., Pearce, F.R., & Scoccimarro, R., 2016, *JCAP* 04, 047
- Smith, R. E., Peacock, J. A., Jenkins, A., et al. 2003, *Mon. Not. Roy. Astron. Soc.* 341, 1311
- Sunayama, T., Padmanabhan, N., Heitmann, K., Habib, S., & Rangel, E., 2016, *JCAP* 05, 051
- Takahashi, R., Sato, M., Nishimichi, T., Taruya, A., & Oguri, M., 2012, *ApJ* 761, 152
- Upadhye, A., Biswas, R., Pope, A., Heitmann, K., Habib, S., Finkel, H., Frontiere, N., & Pope, A. 2014 *Phys. Rev. D* 89, 103515
- Viel, M. Haehnelt, M.G., & Springel, V., 2010, *JCAP* 1006, 015
- Zentner, A.R., Semboloni, E., Dodelson, S., Eifler, T., Krause, E., & Hearin, A. 2013, *Phys. Rev. D* 87, 043509